Pharm Res (2011) 28:2447–2457
DOI 10.1007/s11095-011-0471-0

RESEARCH PAPER

Theoretical Analysis of Interplay of Therapeutic Protein Drug and Circulating Soluble Target: Temporal Profiles of 'Free' and 'Total' Drug and Target

Cuyue Tang • Thomayant Prueksaritanont

Received: 30 January 2011 / Accepted: 3 May 2011 / Published online: 26 May 2011

ABSTRACT

Purpose To systemically investigate, for a therapeutic protein with a circulating soluble target, how the interplay of target dynamics and drug pharmacokinetics defines the 'total' and 'free' drug and target temporal profiles.

Method By extending the established rapid-binding target-mediated drug disposition (TMDD) pharmacokinetic model to circulating soluble targets, the temporal profiles of 'total' and 'free' drug and target were simulated with varying binding affinity (K_D), target baseline (R_{ss}), target turnover, and drug dose level. Two sets of published experimental data were compared with the simulated results.

Results Binding to a circulating soluble target could lead to a divergence of the 'free' drug from the 'total' drug. Simulations show this divergent magnitude determined by K_D and R_{ss}, with the temporal profile being defined by target turnover and drug dose level. As divergence proceeds, starting at the distribution phase, 'free' drug would decline faster but eventually parallel 'total' drug at the terminal phase, giving rise to a steeper distribution phase and comparable terminal half-life, relative to the 'total' form. The model also allows for estimation of the dynamic change of 'total' and 'free' target in response to the treatment of a therapeutic protein drug, facilitating dose level and regimen design to achieve desired 'free' target suppression. Model predictions compared favorably with two sets of published experimental data.

Conclusions Theoretical analyses identified key variables governing the different temporal profiles of 'total' and 'free' drug and target. The rapid-binding TMDD model reasonably captured the features of the interplay of drug pharmacokinetics and target dynamics for two reported cases.

KEY WORDS pharmacodynamics · pharmacokinetics · soluble target · target mediated drug disposition · therapeutic protein drug

ABBREVIATIONS

C	free drug concentration
C_{tot}	total drug concentration
K_D	dissociation constant
PD	pharmacodynamics
PK	pharmacokinetics
R	free target concentration
RB-TMDD	rapid binding approximation of TMDD model
RC	target-drug complex
R_{ss}	target baseline concentration.
R_{tot}	total target concentration
TMDD	target-mediated drug disposition

INTRODUCTION

Therapeutic protein drugs, especially therapeutic monoclonal antibodies, exert their therapeutic activities through highly specific binding to targets. This binding often influences or even dominates their pharmacokinetic (PK) properties, usually manifested as nonlinear PK due to binding saturation of a given target. For instance, exposure-dependent decrease of steady-state volume of distribution has been observed with many biologic drugs (1). For cell-associated targets (usually receptors), located either in the tissue or in the circulation, binding of a drug may be accompanied by internalization of the drug-target complex followed by degradation in endo-

C. Tang (✉) • T. Prueksaritanont
Department of Drug metabolism and Pharmacokinetics
WP75A-203, Merck Research Laboratories
West Point, Pennsylvania 19486, USA
e-mail: cuyue_tang@merck.com

somes or lysosomes, thus rendering another elimination pathway of the drug. The impact of this pathway, usually at a higher rate compared with non-selective systemic elimination, becomes evident when the drug approaches a certain low level where this pathway becomes dominant, leading to altered slopes of the concentration-time curves (2,3). As long as the targets of this class remain bound to the membrane of cells, the drug in the cell-free serum or plasma is conceptually 'free.' In contrast, binding to soluble targets in the circulation, such as cytokines and β-amyloid monomers/oligomers, will engender co-existence of 'free' drug and drug-target complex ('bound') in the circulation. These two forms of drug are also present in serum and plasma where drug exposures are usually measured for PK characterization. Thus, the PK of a therapeutic protein drug can be characterized based on either the 'free' or the 'total' (free + bound) exposure. The case also holds true for the target. However, the 'free' target level usually is too low to be accurately measured, especially in the presence of a drug that has a strong affinity to the target. Thus, the 'total' target is the species in some circumstances to be monitored as the indication of the drug action. This occurrence unique to binding to circulating soluble targets has presented a challenge in the choice of analytical methods as well as data interpretation with respect to the pharmacokinetic and pharmacodynamic relevance, as highlighted in the recent white paper dealing with bioanalytical approaches to quantify 'total' and 'free' therapeutic antibodies and their targets (4).

A key question to be addressed prior to dealing with the aforementioned challenge is how binding to a soluble target would impact the 'free' and 'total' drug PK in terms of magnitude and time-course. In many cases, soluble targets in the circulation are found at low or even undetectable levels. Their impact on drug PK cannot be estimated under static conditions, such as measuring a 'free' or 'total' drug which was spiked into serum or plasma samples from healthy volunteers or patients. However, considerable soluble targets turn out to have rapid production coupled with quick clearance to maintain a low baseline. On the other hand, the concentration of an administered drug in the circulation also changes at a elimination rate usually much slower relative to the target, especially in the case of monoclonal antibodies. It can be envisioned that a potent and specific binding will lead to 1) reduction of the free target which would gradually bounce back, 2) decrease of the free drug which would achieve equilibrium with the total drug, and 3) formation of a drug-target complex which may rise first and then decline in parallel to drug elimination. Conceptually, the magnitude and temporal profiles of these processes are defined by the binding affinity, drug pharmacokinetics and target dynamics. Clearly, quantitative evaluation of this intricate interplay would be greatly facilitated with a mechanism-based model.

A pioneer work in this regard is the PK/PD modeling of accumulation of the complex of an antibody (humanized anti-Factor IX) and Factor IX (a soluble blood borne endogenous antigen) in rats (5). This model well described the time-course of the total antibody, target and antibody-target complex in rats (5), cynomolgus monkeys (6) and humans (7). Subsequently, Mager and Jusko introduced target-mediated drug disposition (TMDD) model to delineate the effect of target binding on drug disposition (8). This model has been widely applied in the field of biologics. Recently, several versions using approximation have been proposed (9–11), including the rapid-binding approximation of TMDD model (RB-TMDD), which replaces the inestimable binding micro-constants (k_{on} and k_{off}) with an equilibrium dissociation constant (K_D). The RB-TMDD model has been applied to some preclinical and clinical studies where the target is membrane-bound receptor (12) or the binding takes place interstitially (13), but its application to circulating soluble targets just started to emerge (14). In fact, the latter case may be better depicted by this model because the encounter of a drug with a target in the circulation would negate distribution of the drug to a binding site outside the vasculature. Unlike a cell-associated drug-target complex, a circulating drug-target complex can be readily measured quantitatively, allowing for experimental evidence for model validation. Another difference is the fate of the complex. Obviously, internalization may not serve as the predominate avenue for a circulating complex, as opposed to a cell-associated one. As such, three scenarios can be envisioned for a circulating complex: 1) the complex is inert; its elimination proceeds through dissociation to 'free' drug and 'free' target; 2) the complex is cleared at the same elimination rate as 'free' drug; that drug disposition remains the same upon binding to a target; 3) the complex is eliminated faster than the 'free' drug. In this work, using the RB-TMDD model, we simulated 'free' and 'total' PK of human IgG-like drugs directing toward a circulating soluble target with different binding and dynamic profiles in three aforementioned scenarios. We also evaluated the dynamic change of 'total' and 'free' target in response to the treatment of a drug at varying dose levels. Finally, we applied this model to describe two sets of published experimental data. One deals with different PK profiles of 'free' and 'total' VEGF Trap upon binding to circulating VEGF in SCID mice (15), and another the time-course of the total β-amyloid 40 (Aβ40) following the administration of a humanized monoclonal antibody solanezumab to patients with mild to moderate Alzheimer's disease (16).

METHODS

PK Model for Simulation

Plasma concentration-time profiles of a drug were simulated using the RB-TMDD model. In this model, free drug in the central compartment (C) is directly eliminated at a first-order rate (k_{el}) or is distributed to a nonspecific tissue-binding site by first-order processes (k_{pt} and k_{tp}). Free target (R) is synthesized at a zero-order rate (k_{syn}) and degraded at a first-order rate (k_{deg}). In addition, C binds to R to form drug-target complex (RC). The binding process is governed by the equilibrium dissociation constant K_D.

$$C + R \xleftrightarrow{K_D} RC; \quad \frac{C \cdot R}{RC} = K_D \tag{1}$$

In addition to dissociation, the complex RC may follow other processes to be eliminated. Different from cell-associated RC, which is likely subjected to internalization, a process denoted k_{int}, an RC of drug and soluble target formed within the circulation may be cleared by other mechanisms. Nevertheless, k_{int} was still used to describe those mechanisms for consistency. The system of differential equations that describes the PK model is as follows:

$$\frac{dC_{tot}}{dt} = In(t) - \left(k_{el} + k_{pt} - k_{int}\right) \cdot C - k_{int} \cdot C_{tot} + k_{tp} \cdot \frac{A_T}{V_c} \tag{2}$$

$$\frac{dA_T}{dt} = k_{pt} \cdot C \cdot V_c - k_{tp} \cdot A_T \tag{3}$$

$$\frac{dR_{tot}}{dt} = k_{syn} - \left(k_{int} - k_{deg}\right) \cdot \left(C_{tot} - C\right) - k_{deg} \cdot R_{tot} \tag{4}$$

where C_{tot} is the total drug concentration ($C_{tot} = C + RC$), R_{tot} is the total target concentration ($R_{tot} = R + RC$), and V_c and A_T denote the apparent volume of the free drug compartment and the amount of the drug outside the vasculature through non-specific distribution, respectively. The input rate ($In(t)$) to the drug compartment accounts for any process that may require additional model component. The target synthesis rate can be calculated from the baseline equation $k_{syn} = k_{deg} \cdot R_{ss}$, where R_{ss} is the baseline of the target at steady state. The free drug C in the circulation is defined by the solution to the following quadratic equation:

$$C = \frac{\left(C_{tot} - R_{tot} - K_D\right) + \sqrt{\left(C_{tot} - R_{tot} - K_D\right)^2 + 4 \times K_D \cdot C_{tot}}}{2} \tag{5}$$

Assuming no endogenous drug production, the initial conditions for the above systems can be defined as follows: $C_{tot}(0) = Dose/V_c$ for bolus intravenous administration, or $C_{tot}(0) = 0$ for other routes of administration: $A_T(0) = 0$; $R_{tot}(0) = R_{ss}$.

Parameter Setting and Simulation

The k_{el} and non-specific distribution parameters V_c, k_{pt} and k_{tp} were fixed to represent the general properties of human (ized) IgG drugs, such as bapineuzumab (17). The parameters that varied in simulations include $Dose$, K_D, R_{ss}, k_{deg}, and k_{int}. For simplicity, all simulations were conducted with intravenous bolus administration, and the binding was set to follow 1:1 stoichiometry (one target binds to one binding site of the drug). In addition, the potential of feedback (changes in the target synthesis rate due to drug treatment) was not considered. The $Dose$, K_D, k_{deg} and R_{ss} varied to evaluate their impact on the temporal profiles of free and total drug as well as target. As for k_{int}, three scenarios were assumed that account for 1) $k_{int}=0$, indicating that the complex RC is stable, and only the free drug is eliminated *via* nonspecific routes; 2) $k_{int}=k_{el}$, suggesting that the target binding does not change the disposition of the drug; thus, the complex RC is eliminated at the same rate as the free drug *via* nonspecific routes; and 3) $k_{int}>k_{el}$, designating a situation where the complex RC can be consumed by additional mechanisms. The symbols and definitions of parameters and variables are presented in Table I. A user-specified RB-TMDD model was developed for computer simulations with WinNonlin (WinNonlin Professional version 5.2.1, Pharsight, Mountain View, CA). Figure 1 shows a representative simulated result of temporal profiles for five variables (C_{tot}, C, R_{tot}, R, and RC) with an intravenous bolus dose of 1 nmol/kg. The parameters for the simulation of different scenarios are listed in Table II. Noticeably, R_{tot} coincides with RC wherever R is much lower than C; hence, R_{tot} serves as a surrogate for RC. The temporal profiles of R_{tot} and RC only diverge from each other when R becomes a major fraction in R_{tot}.

Fitting to Experimental Data

The predictions by the rapid-binding TMDD model with k_{el} being equal to k_{int} were compared with the experimental results of two published cases. One case deals with VEGF Trap complex formation in SCID mice where the 'free' and 'total' drug (VEGF Trap) as well as the complex levels are available (15). Another one concerns the passive immunization with a humanized monoclonal antibody solanezumab targeting β-amyloid monomers. In a clinical trial, solanezumab and total Aβ40 were measured (16). In both cases, the mean concentration values were digitized (Graph Digitizer version 9.1) from the published results.

Table I Symbols and Definitions of Parameters and Variables Used in Simulation with Rapid-binding TMDD Model

Parameter (unit)	Definition
k_{el} (h^{-1})	First-order elimination rate constant
k_{pt} (h^{-1})	First-order distribution rate constant from plasma to peripheral sites
k_{tp} (h^{-1})	First-order distribution rate constant from peripheral sites to plasma
k_{deg} (h^{-1})	First-order target degradation rate constant
K_D (nM)	Equilibrium dissociation constant
k_{int} (h^{-1})	First-order rate constant for elimination of drug-target complex RC
R_{ss} (nM)	Target baseline concentration (steady state concentration in the absence of drug)
V_c (L/kg)	Volume of the central plasma compartment
C_{tot} (nM)	Total drug concentration in the circulation
C (nM)	Free drug concentration in the circulation
R_{tot} (nM)	Total target concentration in the circulation
R (nM)	Free target concentration in the circulation
RC (nM)	Drug-target complex concentration in the circulation

As for VEGF Trap, the PK parameters (k_a, k_{el}, k_{pt}, k_{tp}, V_c) of the total drug were first estimated *via* the built-in two-compartmental model in WinNonlin for each dose group. Based on these initial estimates, together with the information on binding affinity (K_D) and target dynamics ($t_{1/2}$ and R_{ss}), data fitting for free and total VEGF Trap and the complex concentrations were optimized.

In the case of solanezumab, its clearance was derived from the drug AUC reported. As distribution parameters are not available, average values for human IgG monoclonal antibody drugs were used. The affinity of this drug to soluble Aβ monomers has been reported to be high. Thus, the K_D was set to be 0.1 nM. The baseline of Aβ40 reported in literature is less than 1 nM in most cases. The range obtained from a recent clinical trial is 60 to 90 pM (300–400 pg/mL) in humans (18). Thus, the concentration of 80 pM was used as R_{ss} for the simulation. The Aβ monomers have been known to be eliminated fast. For instance, the $t_{1/2}$ of the injected Aβ40 is reported to be approximately 10 min in rodents (19). Similarly, based on these estimates, the predicted total Aβ40 time-course following the treatment of solanezumab at different doses was compared with the observed profiles. The parameter values for simulations in these two cases are listed in Table III.

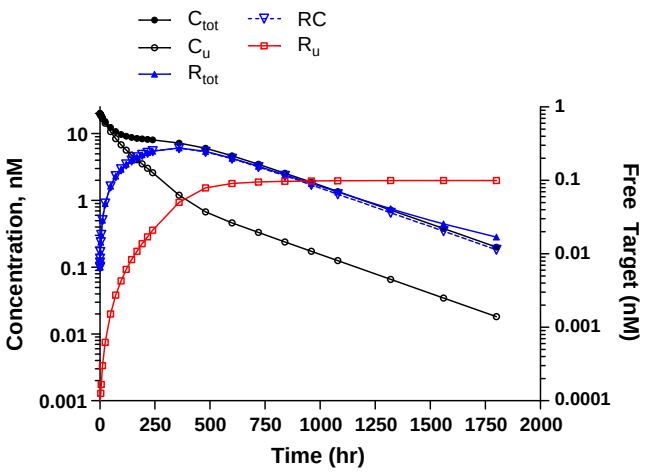

Fig. 1 Representative simulated temporal profiles of five variables (C_{tot}, C, R_{tot}, R, and RC) with an intravenous bolus dose of 1 nmol/kg. The values of parameters used for the simulation are listed in Table II.

RESULTS

The Effect of Binding Affinity

To analyze the impact of binding affinity on 'free' and 'total' drug PK, three K_D values (1, 0.1, and 0.01 nM) are used with fixed dose (10 nmol/kg), R_{ss} (0.1 nM), and k_{deg} (4.158 hr^{-1}, equivalent to a $t_{1/2}$ of 10 min). In this case, the k_{int} is set equal to the k_{el}, mimicking the situation that binding of the target to the drug does not change drug elimination. As depicted in Fig. 2, binding to a target changes the distribution phase of both C and C_{tot}. Relative to the PK profile of the drug in the absence of soluble target binding, the distribution phase of the C becomes steeper as binding affinity increases or K_D decreases. The opposite is seen with the C_{tot}, i.e., the increase of the affinity leads to a shallower distribution phase. When the affinity is very high (K_D=0.01 nM), the C_{tot} displays a slight rise after the first drop. This may be attributed to the redistribution of the drug from tissues back to the circulation, as this rise in the C_{tot} disappears upon reducing tissue distribution by 10-fold (k_{pt}=0.001 hr^{-1}) (data not shown). Clearly, the additional distribution depot generated by binding to the soluble target sets the C apart from the C_{tot}. As the distribution phase of the C may be steeper and last longer relative to the C_{tot}, insufficient sampling or limited assay sensitivity may erroneously give rise to a shorter $t_{1/2}$ for the C than for the C_{tot}.

As the disposition proceeds toward terminal phase, the C starts to decline in parallel to the C_{tot} with a ratio defined by the affinity. Namely, the terminal $t_{1/2}$ of both forms is identical. This observation holds true in any condition, as demonstrated in the following cases. Noticeably, relative to the situation without target binding, the elimination of both C and C_{tot} becomes faster in the presence of target binding in an affinity-dependent manner: the lower the K_D, the steeper the terminal phase. This could be accounted for by the decrease of volume of distribution because increased

Table II Values of Parameters Used in Simulation with Rapid-binding TMDD Model in Different Cases

Case	k_{el} (hr^{-1})	k_{pt} (hr^{-1})	k_{tp} (hr^{-1})	k_{deg} (hr^{-1})	K_D (nM)	k_{int} (hr^{-1})	R_{ss} (nM)	V_c (L/kg)	Dose (nmol/kg)
Fig 1	0.003	0.01	0.01	0.3456	0.01	0.0012	0.1	0.05	1
Fig 2	0.003	0.01	0.01	4.518	Varying	0.0012	0.1	0.05	10
Fig 3A	0.003	0.01	0.01	4.518	0.1	0.0012	Varying	0.05	10
Fig 4	0.003	0.01	0.01	Varying	0.1	0.0012	0.1	0.05	10
Fig 5	0.003	0.01	0.01	4.518	0.1	0.0012	0.1	0.05	Varying
Fig 6	0.003	0.01	0.01	4.518	Varying	0	0.1	0.05	10
Fig 7	0.003	0.01	0.01	4.518	Varying	0.015	0.1	0.05	100

binding to a target in the circulation would theoretically reduce the distribution to tissues, leading to a smaller volume of distribution.

The Effect of Target Baseline and Turnover

The simulated result illustrated in Fig. 3a indicates that with a fixed K_D, a higher R_{ss} leads to a greater C_{tot}/C ratio at the terminal phase. This figure delineates the C_{tot} and C temporal profiles in the presence of a relatively fast turnover target ($t_{1/2}$ of 10 min) with the R_{ss} of 0.1 or 0.5 nM (K_D=0.1 nM; dose=10 nmol/kg). The C_{tot}/C ratios at the terminal phase are 2 and 6 for R_{ss} of 0.1 and 0.5 nM, respectively. In fact, both the K_D and the R_{ss} can influence the C_{tot} and C temporal profiles. Although the actual levels of K_D and R_{ss} define the time-course of C_{tot} and C, the C_{tot}/C ratio at the terminal phase is governed by the ratio of R_{ss}/K_D. Namely, regardless of the actual value of R_{ss} and K_D, the higher the ratio, the greater the difference between C_{tot} and C. Predictions by the model showed a linear relationship between R_{ss}/K_D and C_{tot}/C, which is outlined in Fig. 3b. This relationship could facilitate reasonable estimation of the difference between C_{tot} and C. According to the prediction, no significant difference would be expected for C_{tot} and C when the R_{ss}/K_D ratio is less than 0.25 (C_{tot}/C ratio of 1.25). This result clearly indicates that the binding affinity and target baseline are important determinants of the magnitude of C_{tot} and C divergence.

Table III Parameter Values for Simulations in the Cases of VEGF Trap and Solanezumab

Parameter	VEGF Trap (15)	Solanezumab (16)
k_{el} (h^{-1})	0.021	0.002
k_{pt} (h^{-1})	0.002–0.009	0.002
k_{tp} (h^{-1})	0.004	0.002
k_{deg} (h^{-1})	8.316	2.079
K_D (nM)	0.001	0.1
k_{int} (h^{-1})	0.021	0.002
R_{ss} (nM)	0.02	0.08
V_c (L/kg)	0.06–0.074	0.05
Dose (mg/kg)	1, 2.5, 10, 25	0.5, 1.5, 4, 10

It is important to point out that the difference between C_{tot} and C observed in a PK study may be underestimated by an *in vitro* experiment where plasma/serum samples are spiked with a drug to determine target interference. The total target concentration R_{tot} in those samples is equivalent to the R_{ss} *in vivo*. However, the *in vitro* study neglects the continuous production of the target, a process whose impact can only manifest *in vivo*. For instance, based on receptor-ligand binding equilibrium, the calculated C_{tot}/C ratio is 2.79 with K_D, R_{tot} and C_{tot} of 0.1, 0.5 and 0.5 nM, respectively, while the ratio derived from a PK study turns out to be 6 with K_D and R_{ss} of 0.1 and 0.5 nM (Fig. 3b). Another significant difference is that the C_{tot}/C ratio *in vitro* would vary with C_{tot} as R_{tot} is a constant. As C_{tot}/R_{tot} decreases, the C_{tot}/C ratio increases. When C_{tot} is in large excess of R_{tot}, the ratio approaches unity. In contrast, the incessant supply of the target to the circulation shifts the C_{tot}/C ratio *in vivo* until all species reach the equilibrium which is governed by the affinity. Therefore, the C_{tot}/C ratio stays constant over a wide range of drug concentration.

The baseline of a target R_{ss} is determined by its production and degradation ($R_{ss}=k_{sym}$ / k_{deg}). For a given R_{ss}, k_{syn} and k_{deg} could vary, but the net effect can be indicated by the target half-life ($t_{1/2}$), or target turnover. Figure 4 illustrates the impact of target turnover on the temporal profiles of drug and target. With a given R_{ss} (0.1 nM), a faster turnover target ($t_{1/2}$=5 min, Fig. 4a) leads to a steeper distribution phase of C and a quick recovery of the free target R than a slower turnover target ($t_{1/2}$=120 min, Fig. 4b). Obviously, within a same timeframe, more targets are synthesized if the turnover is faster and thus consume the drug faster. However, the C_{tot}/C ratio at the terminal phase is not influenced by the turnover. As mentioned above, this ratio is determined by K_D and R_{ss} only. Of significance is the time-course of R_{tot} in relation to R at different target turnover rates. In the case of a quick turnover target (Fig. 4a), R

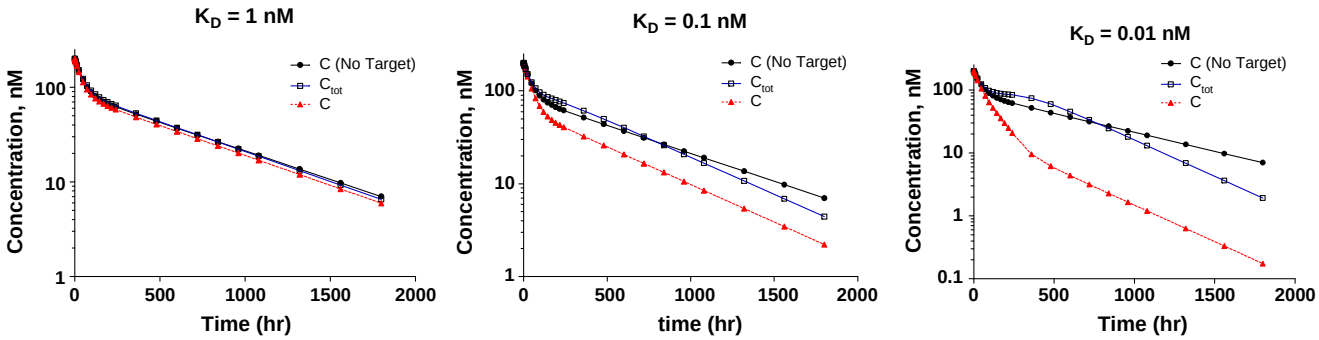

Fig. 2 Simulated temporal profiles of 'total' and 'free' drug with different binding affinity. The values of parameters used for the simulation are listed in Table II. The results suggest that the difference of C_{tot} and C increases as K_D decreases.

bounces back to 50% of R_{ss} prior to 72 hr post-dose, while R_{tot} hits its peak (~ 44 nM, i.e. 440-fold higher than R_{ss}) at approximately 120 hr when R has been almost back to R_{ss}. On the contrary, it takes 960 hr for R to return to 50% of R_{ss} when the target $t_{1/2}$ is 120 min (Fig. 4b). Meanwhile, a lower R_{tot} peak level (8 nM) arrives around 720 hr. Therefore, in both cases R_{tot} does not reflect R well in the temporal profile.

The Effect of Dose Level

Three dose levels (1, 10 and 100 nmol/kg) are included to evaluate the 'free' and 'total' drug and target temporal profiles with the target $t_{1/2}$ being set 10 min. The results are shown in Fig. 5. As K_D of 0.1 nM and R_{ss} of 0.1 nM are used in all cases, the C_{tot}/C ratio at the terminal phase therefore remains the same (2-fold) at all dose levels. However, the speed at which C departs from C_{tot} is dose-dependent (Fig. 5d). Thus, the time required for C to drop to 25% of C_{tot} is approximately 12, 90 and 700 hr for the 1, 10 and 100 nmol/kg doses, respectively. This observation can be reasonably explained by the ratio of drug to the target. Since a fraction of C_{tot} in the circulation will bind the target which is formed at a constant rate, a greater fraction of C_{tot} would be consumed faster for a lower dose, leading to an early departure of C from C_{tot}. The opposite can be expected for a higher dose. This finding is in good agreement with the work by Beningcosa *et al.* for a humanized anti-Factor IX antibody in cynomolgus monkeys (6).

Of note is the dose-response of target change. As for the total target R_{tot}, both the maximal concentration and peak time increases with drug dose level, as depicted in Fig. 5e. Especially at the 100 nmol/kg dose, the slow rise of the R_{tot} significantly has delayed its terminal phase. This is consistent with the departure rate and magnitude of C from C_{tot} described above. Davis *et al.* have reported a drug dose-dependent target accumulation in the circulation (5), an observation similar to our predicted result. With respect to the R change (the indication of pharmacological effect), the magnitude and duration of its suppression increase with the drug dose (Fig. 5f). Again, the R has already bounced back, while the total target R_{tot} is still > 100-fold higher than the baseline target level.

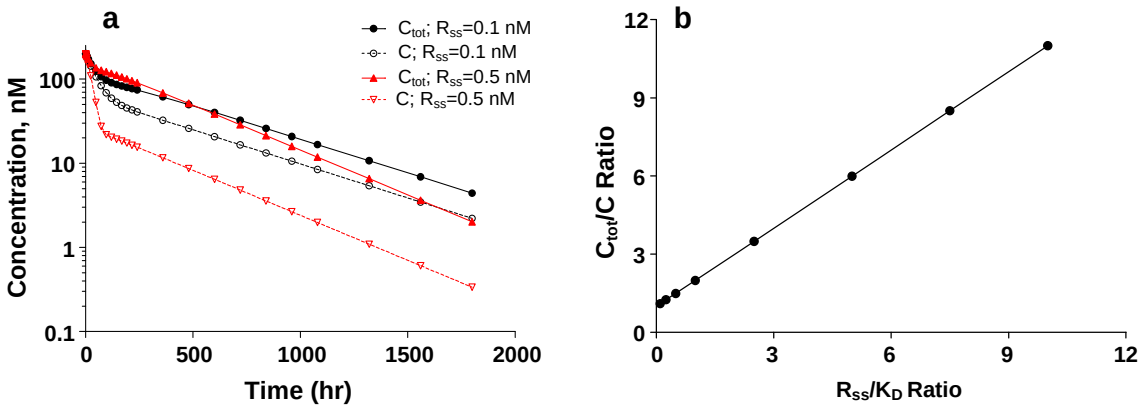

Fig. 3 (**a**) Simulated temporal profiles of 'total' and 'free' drug with different R_{ss} levels. The values of parameters used for the simulation are listed in Table II. (**b**) The ratio of 'total' and 'free' drug concentration at the terminal phase (C_{tot}/C) *versus* the ratio of R_{ss}/K_D. The results indicate that the ratio of R_{ss}/K_D determines the magnitude of the difference between C_{tot} and C at terminal phase.

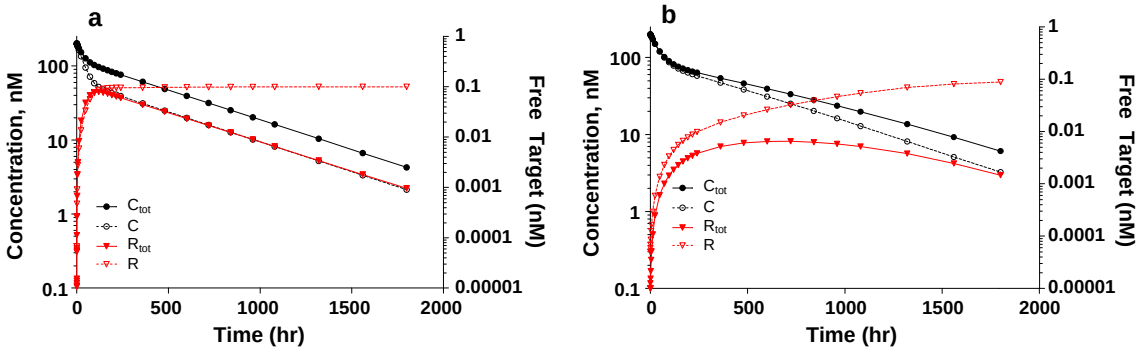

Fig. 4 Simulated temporal profiles of 'total' and 'free' drug and target with a fast turnover target (**a**, target $t_{1/2}$ of 5 min) and a slow turnover target (**b**, target $t_{1/2}$ of 120 min). The values of other parameters used for the simulation are listed in Table II. The results demonstrate that at a given drug dose, the quicker the turnover of the target, the sooner the departure of *C* from C_{tot}.

The Effect of Drug-Target Complex RC Elimination

In the above cases, the complex *RC* is set to be eliminated identically as the free drug *C* ($k_{el}=k_{int}$). Now we examine two situations: $k_{int}=0$ and $k_{int}=5\ k_{el}$. The first scenario is the extreme case of situations where *RC* is more stable than *C*, while the second one represents the events where *RC* is eliminated faster than *C via* additional routes. Analyses are performed with varying K_D values. In the second scenario, a higher dose (100 nmol/kg) is chosen to allow for saturation of the pathway governed by k_{int}. As depicted in Fig. 6, when dissociation is the only route to reduce *RC*, the terminal elimination rate of both C_{tot} and *C* declines with the affinity. This simulated result may be rationalized by the formation of a more stable *RC* which reduces the fraction of *C* subjected to elimination. On the contrary, if k_{int} is five times greater than k_{el}, a typical TMDD profile appears when K_D is $\leq$ 0.1 nM, as evidenced by the downward change of the slope when drug concentration has dropped to approximately 100 nM (Fig. 7). Clearly, this phenomenon is dose-dependant. The dose should be high enough to saturate the route governed by k_{int} first. Otherwise, the overall elimination process would be controlled by k_{int}. In both scenarios, the ratio of C_{tot}/C at the terminal phase is determined by the K_D and R_{ss}, similar to aforementioned cases.

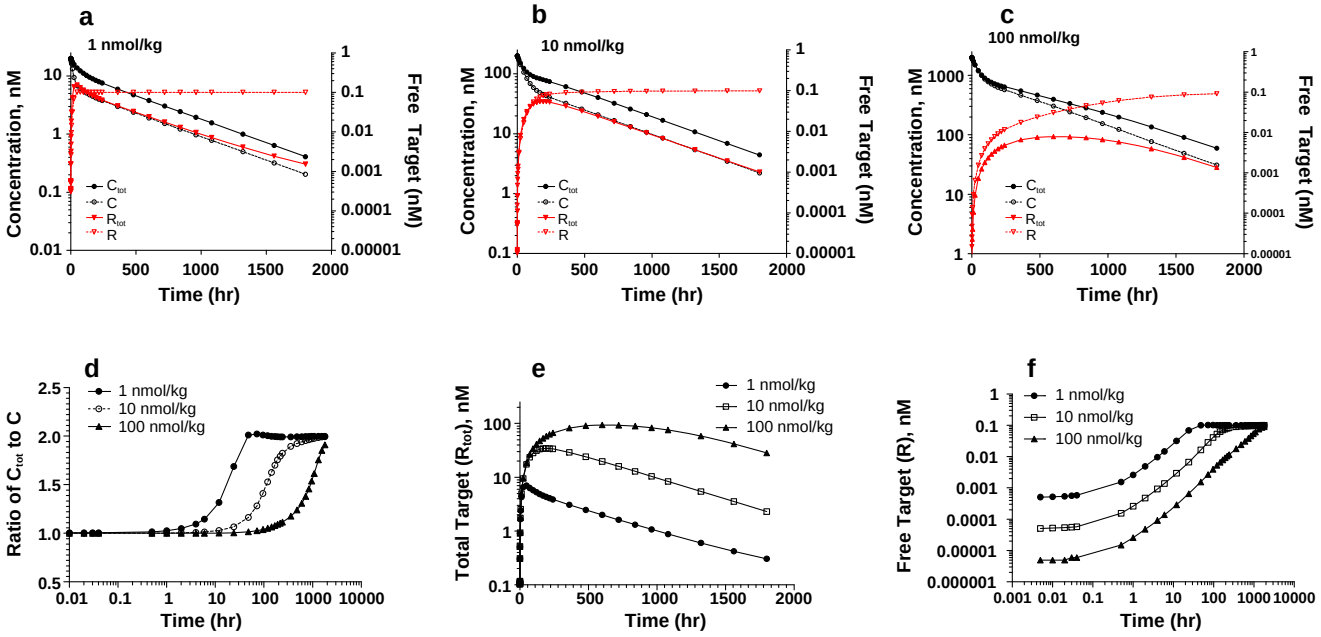

Fig. 5 Simulated temporal profiles of 'total' and 'free' drug at three dose levels (**a**, **b**, **c**). The time-course of C_{tot}/C ratio, complex concentration (*RC*) and free target concentration (*R*) are depicted in figures **d**, **e** and **f**, respectively. The values of parameters used for the simulation are listed in Table 2. The results indicate that, for a given K_D and R_{ss}, the drug dose level determines the rate of *C* deviation from C_{tot}, the maximal level of complex *RC* and the time to achieve it, and the duration of target suppression.

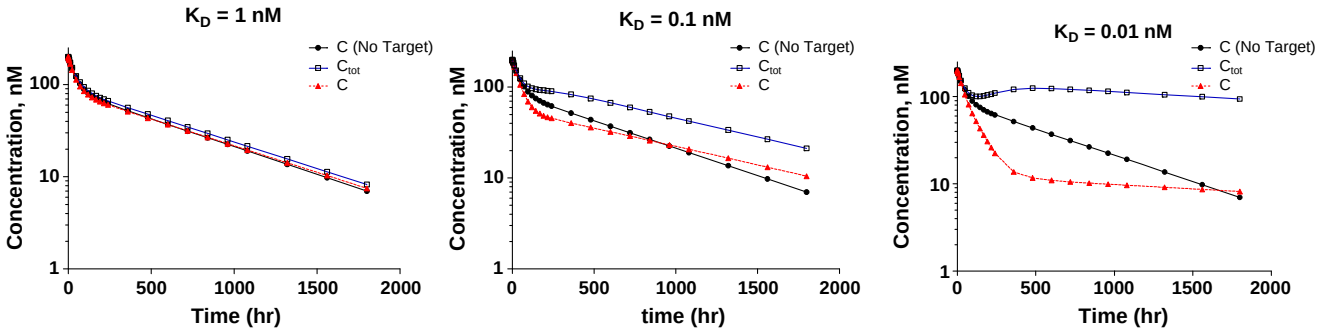

Fig. 6 Simulated temporal profiles of 'total' and 'free' drug with different binding affinity when the complex *RC* is not subject to elimination ($k_{int} = 0$). The values of other parameters used for the simulation are listed in Table II. The results indicate that when only the bound drug can be eliminated, the affinity determines not only the magnitude of the difference between C_{tot} and C, but also drug elimination rate.

Model Validation with Two Sets of Published Experimental Data

While no comprehensive experimental data are available to fully validate the features described by the RB-TMDD model for soluble targets in the circulation, attempts have been made to qualitatively confirm the temporal profiles of C_{tot}, C and R_{tot} by comparing model calculations with two sets of published experimental data. The first one is the dose-dependent temporal divergence between free and total VEGF Trap as well as total VEGF in SCID mice (15). The second one is the time-course of total Aβ40 at different doses of solanezumab (a humanized monoclonal antibody with a high affinity toward human Aβ40) in patients with mild to moderate Alzheimer's disease (16).

In the case of VEGF Trap, which binds to VEGF in the circulation with a high affinity (K_D<1 pM) to form a complex, most of the injected VEGF Trap is initially found in free form, but after reaching peak levels the free form in the circulation declines progressively. The departure of the free form from the total drug starts sooner at lower doses with a steeper slope (15). This is consistent with the simulation described in Fig. 5d. As the clearance of free and bound VEGF Trap is reported to be identical (15), the k_{int} is set equal to the k_{el} for simulations. Encouragingly, strong qualitative agreement between the simulated data and experimental data are observed (Fig. 8). For example, the estimated K_D of 1 pM and VEGF $t_{1/2}$ of 5 min are consistent with the reported range (K_D<1 pM and $t_{1/2}$ of only minutes). In addition, the estimated VEGF baseline (0.02 nM) is also falling into the range of reported value (0.04 to 1 ng/mL=0.001 to 0.025 nM). The model has also well captured the time-course of the complex in terms of the time taken to reach the peak, duration of the plateau, and decline rate for each dose (Fig. 9a). While the peak level is somewhat underestimated by 50–100% for the two high doses (10 and 25 mpk), both the experimental data and the model-predicted results suggest no further significant increase of complex peak level within the dose range tested. This plateau of the complex formation is anticipated when free VEGF Trap is in excess of the complex (15). However, in general, the free drug concentration is not the only factor. Further analyses indicated that at a given dose it is more readily to achieve and maintain the maximal *RC* level for a target of low K_D, k_{deg} and R_{ss} than the opposite (data not shown). The next case may reflect this notion *via* the time-course of total target.

The baseline of Aβ40 is reported to be around 0.1 nM, 5-fold higher than the estimated VEGF baseline. The peak levels of total Aβ40 increases with the dose of solanezumab,

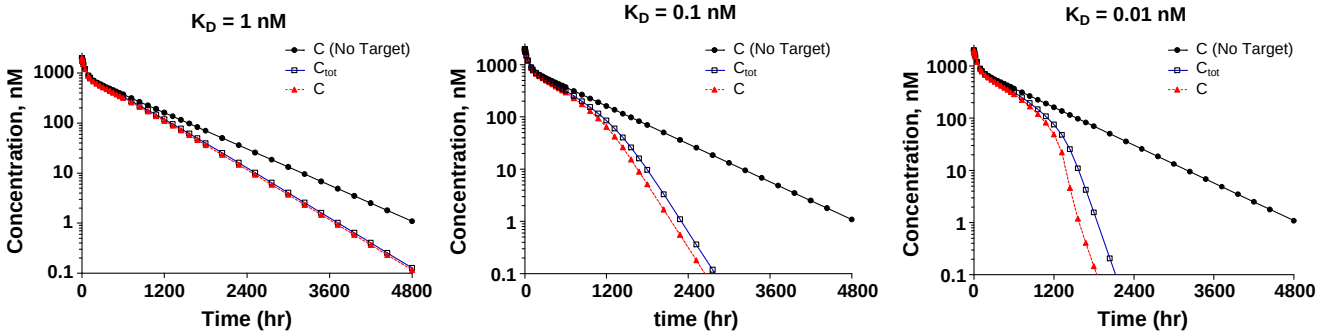

Fig. 7 Simulated temporal profiles of 'total' and 'free' drug with different binding affinity when the complex *RC* is eliminated 5-fold faster than the 'free' drug ($k_{int} = 5\ k_{el}$). The values of other parameters used for the simulation are listed in Table II. The results suggest that when complex *RC* is eliminated faster than the free drug *C*, the higher the affinity, the sooner the change of elimination rate displays.

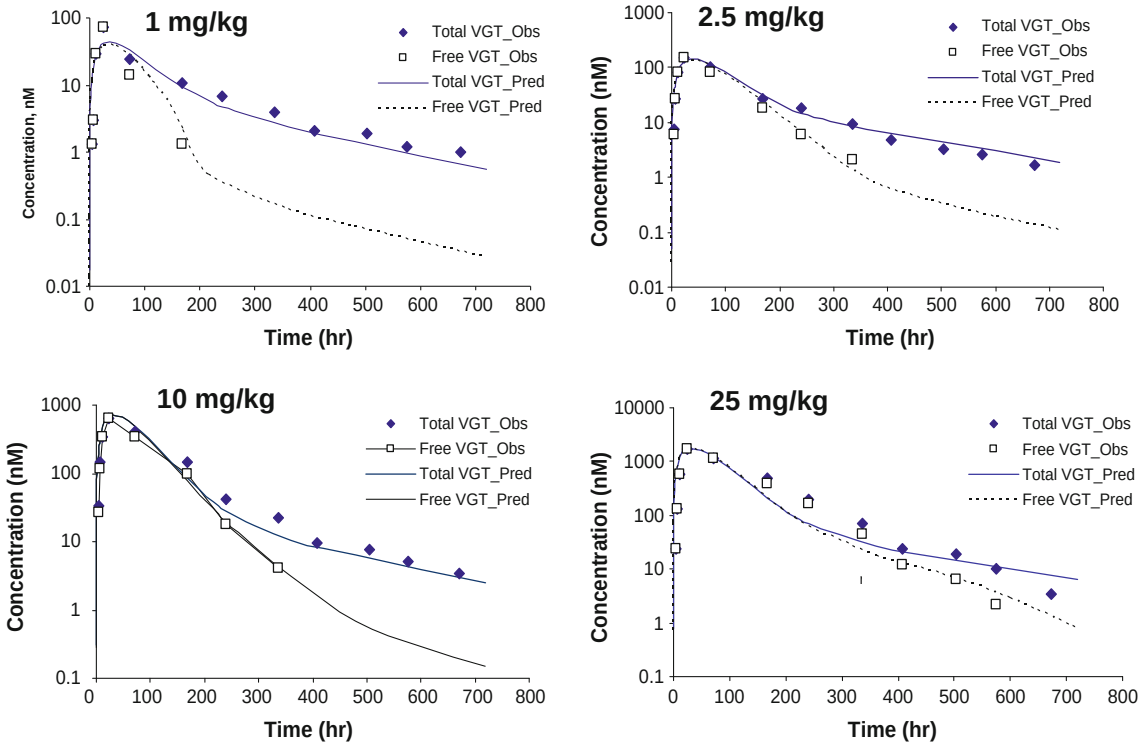

Fig. 8 The time-course of circulating total and free VEGF Trap (VGT) in SCID mice following intravenous administration of different doses. Lines represent predicted profiles from fitting the rapid-binding TMDD model. The values of parameters used for prediction are listed in Table III. The results demonstrate that the RB-TMDD model reasonably describes the PK profile of total and free VGT.

but in a less dose-proportional manner (16). Once again, these features have been reasonably captured by the RB-TMDD model (Fig. 9b). The estimated K_D (0.1 nM) and R_{ss} (0.08 nM) are in line with the reported values, but the estimated Aβ40 $t_{1/2}$ (20 min) appears to be longer than the most reported values for animals (≤ 10 min). The continuous increase of the peak level of Aβ40 suggests that the complex formation has not reached the maximal level at the given dose range (0.5–10 mg/kg). As predicted by the model (Fig. 5e), the T_{max} of the complex has shifted to the right as the dose rises. Meanwhile, the curve becomes flatter and the terminal phase is delayed at higher doses. As such, insufficient sampling duration may lead to a longer apparent $t_{1/2}$ of the total target which could exceed the

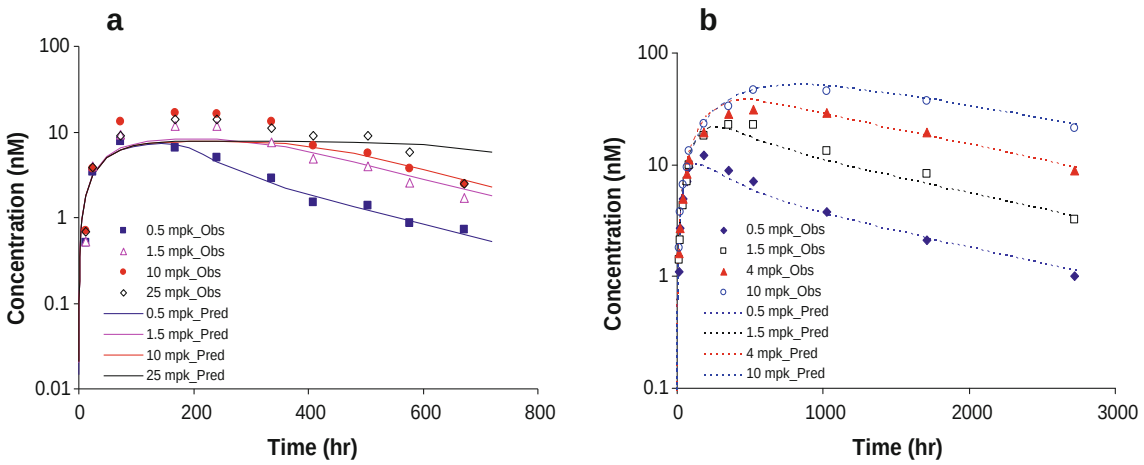

Fig. 9 The time-course of circulating complex of VEGF-VGT in SCID mice (**a**) or solanezumab-Aβ40 in Alzheimer's disease patients (**b**) following intravenous administration of different doses. Lines represent predicted profiles from fitting the rapid-binding TMDD model. The values of parameters used for prediction are listed in Table III. The experimental data are well captured by RB-TMDD model. The result of VEGF-VGT complex illustrates a ready saturation of a target with low R_{ss} and low turnover. The result of solanezumab-Aβ40 complex demonstrates how the drug level influences the temporal profile of the complex and the magnitude of maximal complex prior to saturation of the target binding.

drug terminal $t_{1/2}$ at higher doses. This possibility may reasonably account for the intriguing observation that the $t_{1/2}$ of the total Aβ40 appears to increase with dose (22, 36, 41 and 48 days at 0.5, 1.5, 4 and 10 mg/kg, respectively).

DISCUSSION

In targeting circulating soluble ligands that are associated with disease symptoms when excessively expressed, the efficacy of a drug would be reflected by the magnitude and duration of the free target suppression upon which the drug dose level and regimen are defined. However, monitoring the free target R is very challenging, if not impossible, in the presence of a capturing drug. On the other hand, while it is preferred to measure the free drug C as it directly drives efficacy, the appropriate assay may not be always available. In addition, C could be significantly lower than C_{tot} when the ratio of R_{ss}/K_D is greater than 2. With a mechanism-based model, C_{tot} and R_{tot} in the circulation can be integrated for quantitative simulations for C as well as R. Meanwhile, such a model would offer a good understanding of the interplay of drug pharmacokinetics and target dynamics. In this study, with the rapid-binding TMDD model which has been validated by others, theoretical analyses were performed to identify the key variables that govern how C and R vary relative to the respective total forms.

One of expected outcomes of binding to a soluble target is a lower C than C_{tot}. The analyses indicate that the difference gradually enlarges with time depending on the dose, target dynamics and drug PK, and becomes constant at the terminal phase, indicating an identical terminal $t_{1/2}$ for both forms. The degree of the deviation at the terminal phase (C_{tot}/C ratio) is determined by K_D and R_{ss} at any conditions. Obviously, a high affinity (e.g. K_D of 1 pM) could result in a C more than 10-fold lower than C_{tot} at R_{ss} levels commonly seen for a number of soluble targets (≤ 1 nM). The binding also leads to a steeper distribution phase which lasts longer for C than for C_{tot}. Therefore, caution has to be taken in interpreting the free drug PK because the distribution $t_{1/2}$ may be mistakenly assigned as the terminal $t_{1/2}$ for C if the terminal phase of C were incorrectly defined due to insufficient data points. As the temporal profile of C could be estimated by modeling, this approach will facilitate data interpretation, as exemplified by the work of Xiao *et al.* (14) and our analysis of the free VEGF PK (Fig. 8). Another application of model-based prediction is to assist in assay validation/trouble shooting. For instance, if measured C_{tot} and C differ much more than the predicted degree, efforts should be made to look into potential interfering factors or assay defect. As a general rule, minimal difference between C_{tot} and C is anticipated when the ratio of R_{ss} to K_D is greater than 0.5. In addition, the information can also help optimize sampling time and duration in designing animal and human pharmacology studies.

Binding to mAb drugs to form 1:1 or 2:1 monomeric complex RC will prolong the $t_{1/2}$ of small soluble targets, which otherwise would be cleared fast. The resultant RC in most cases follows free drug C elimination. A good example is plasma Aβ species (16). Characterizing the temporal profile of such RC can provide insights into target dynamics. Rudge *et al.* use RC at the maximal steady state to estimate VEGF production rate and define efficacious dose level and regimen for VEGF Trap (15). Our analyses indicate that in the timeframe where RC is sustained, R suppression is retained >80% (data not shown) in the case of VEGF. However, this approach may be feasible only for a target with a low R_{ss} and/or slow turnover. Otherwise, a considerably high dose would be required to maintain a reasonable duration of sustained RC. By extension, targeting a ligand with high turnover and R_{ss} could be cost prohibitive and thus a consideration factor for target selection from drug discovery/development perspective. In a larger sense, the rate of RC formation and its peak level reflect the target turnover. A quicker rise of RC to a higher peak would indicate a faster turnover at a given dose, but also implies a quicker bounce back of R. As a separate note, heterogeneous multimeric complexes have the propensity to deposit to tissues, such as kidney glomeruli (20), leading to a faster clearance of the complexes relative to the free drug. This occurrence is equivalent to the case of $k_{\mathrm{int}} > k_{\mathrm{el}}$.

Accumulation of either R_{tot} or RC has been monitored in many studies due to technical difficulty in measuring R following drug administration. However, it is critical to put the data in a proper context. The time-course of R_{tot} or RC does not bestow R suppression directly, as suggested by our simulation. Even when RC is sustained, R may already start to rise. In this regard, the model-based predictions would be of great value in linking R_{tot} or RC to R in time-course. Such predictions also shed light on a perplexing observation that $t_{1/2}$ of total Aβ40 increases with the dose level of solanezumab and was longer than the drug $t_{1/2}$ at higher doses (16). As predicted by the model, the peak of R_{tot} or RC gets delayed and the curve becomes broader as drug dose increases until achieving a plateau. However, the true terminal phase of RC should keep tract with that of the drug, either 'total' or 'free.' It is conceivable that limited data points could erroneously define the $t_{1/2}$ of R_{tot} or RC. It should be noted that, relative to the drug $t_{1/2}$, R_{tot} could theoretically display an apparently longer $t_{1/2}$ when R accounts for significant fraction of the R_{tot}. This occurrence may take place at the very terminal phase, especially if R_{ss} is relatively high. Nevertheless, conventional sampling design usually does not include that period, and hence it may not be readily observed.

In summary, using the RB TMDD model, we have predicted the temporal profiles of 'total' and 'free' drug and target under different conditions. These theoretical analyses have provided an improved understanding of the quantitative interplay of the pharmacokinetics of therapeutic protein drugs and the dynamics of soluble targets. The model also well describes some published experimental results and provides mechanistic insights into some observations. The identification of the key variables that govern the difference in total and free drug PK should facilitate assay selection, trouble shooting, and data interpretation. The estimation of the dynamic change of 'total' and 'free' target in response to the treatment of a drug would guide pharmacological studies in the selection of dose level and regimen.

REFERENCES

1. Lobo ED, Hansen RJ, Balthasar JP. Antibody pharmacokinetics and pharmacodynamics. J Pharm Sci. 2004;93:2645–68.
2. Bauer RJ, Gibbons JA, Bell DP, Luo ZP, Young JD. Nonlinear pharmacokinetics of recombinant human macrophage colony-stimulating factor (M-CSF) in rats. J Pharmacol Exp Ther. 1994;268:152–8.
3. Bauer RJ, Dedrick RL, White ML, Murray MJ, Garovoy MR. Population pharmacokinetics and pharmacodynamics of the anti-CD11a antibody hu1124 in human subjects with psoriasis. J Pharmacokinet Biopharm. 1999;27:397–420.
4. Lee JW, Kelley M, King LE, Yang J, Salimi-Moosavi H, Tang MT, *et al.* Bioanalytical approaches to quantify "total" and "free" therapeutic antibodies and their targets: technical challenges and PK/PD applications over the course of drug development. AAPS J. 2011 Jan 15. [Epub ahead of print].
5. Davis CB, Tobia LP, Kwok DC, Oishi CM, Kheterpal N, Hepburn TW, *et al.* Accumulation of antibody-target complexes and the pharmacodynamics of clotting after single intravenous administration of humanized anti-Factor IX monoclonal antibody to rats. Drug Delivery. 1999;6:171–9.
6. Benincosa LJ, Chow FS, Tobia LP, Kwok DC, Davis CB, Jusko WJ. Pharmacokinetics and pharmacodynamics of a humanized monoclonal antibody to factor IX in cynomolgus monkeys. J Pharmacol Exp Ther. 2000;292:810–6.
7. Chow FS, Benincosa LJ, Sheth SB, Wilson D, Davis CB, Minthorn EA, *et al.* Pharmacokinetic and pharmacodynamic modeling of humanized anti-factor IX antibody (SB 249417) in humans. Clin Pharmacol Ther. 2002;71(4):235–45.
8. Mager DE, Jusko WJ. General pharmacokinetic model for drugs exhibiting target-mediated drug disposition. J Pharmacokinet Pharmacodyn. 2001;28:507–32.
9. Mager DE, Krzyzanski W. Quasi-equilibrium pharmacokinetic model for drugs exhibiting target-mediated drug disposition. Pharm Res. 2005;22:1589–96.
10. Marathe A, Krzyzanski W, Mager DE. Numerical validation and properties of a rapid binding approximation of a target-mediated drug disposition pharmacokinetic model. J Pharmacokinet Pharmacodyn. 2009;36:199–219.
11. Gibiansky L, Gibiansky E. Target-mediated drug disposition model: relationships with indirect response models and application to population PK-PD analysis. J Pharmacokinet Pharmacodyn. 2009;36:341–51.
12. Segrave AM, Mager DE, Charman SA, Edwards GA, Porter CJ. Pharmacokinetics of recombinant human leukemia inhibitory factor in sheep. J Pharmacol Exp Ther. 2004;309:1085–92.
13. Marathe A, Peterson MC, Mager DE. Integrated cellular bone homeostasis model for denosumab pharmacodynamics in multiple myeloma patients. J Pharmacol Exp Ther. 2008;326:555–62.
14. Xiao JJ, Krzyzanski W, Wang YM, Li H, Rose MJ, Ma M, *et al.* Pharmacokinetics of anti-hepcidin monoclonal antibody Ab 12B9m and hepcidin in cynomolgus monkeys. AAPS J. 2010 Aug 25.
15. Rudge JS, Holash J, Hylton D, Russell M, Jiang S, Leidich R, *et al.* Inaugural Article: VEGF Trap complex formation measures production rates of VEGF, providing a biomarker for predicting efficacious angiogenic blockade. Proc Natl Acad Sci U S A. 2007;104:18363–70.
16. Siemers ER, Friedrich S, Dean RA, Gonzales CR, Farlow MR, Paul SM, *et al.* Safety and changes in plasma and cerebrospinal fluid amyloid beta after a single administration of an amyloid beta monoclonal antibody in subjects with Alzheimer disease. Clin Neuropharmacol. 2010;33:67–73.
17. Black RS, Sperling RA, Safirstein B, Motter RN, Pallay A, Nichols A, *et al.* A single ascending dose study of bapineuzumab in patients with Alzheimer disease. Alzheimer Dis Assoc Disord. 2010;24:198–203.
18. Raskind M, Liang E, Sperling R, Boxer A, Ross, Brody M, *et al.* Pharmacokinetics and pharmacodynamics of bapineuzumab following multiple intravenous infusions in patients with mild-to-moderate Alzheimer's Disease. Poster P3-246. Presented at the Alzheimer's Association 2009 International Conference on Alzheimer's Disease, 11–16 July 2009, Vienna, Austria. http://www.abstractsonline.com/plan/ViewAbstract.aspx?sKey=ca162e8d-9178-41b0-bf96-04216f4d1083&cKey=af781608-6f44-4030-a5ab-6db76ef92f46
19. Kandimalla KK, Curran GL, Holasek SS, Gilles EJ, Wengenack TM, Poduslo JF. Pharmacokinetic analysis of the blood-brain barrier transport of 125I-amyloid beta protein 40 in wild-type and Alzheimer's disease transgenic mice (APP, PS1) and its implications for amyloid plaque formation. J Pharmacol Exp Ther. 2005;313:1370–8.
20. Gerber HP, Wu X, Yu L, Wiesmann C, Liang XH, Lee CV, *et al.* Mice expressing a humanized form of VEGF-A may provide insights into the safety and efficacy of anti-VEGF antibodies. Proc Natl Acad Sci U S A. 2007;104:3478–83.